A structural study of ceramics in the $(BiMnO_3)_x$–$(PbTiO_3)_{1-x}$ solid solution series

2004 J. Phys.: Condens. Matter 16 8823

(http://iopscience.iop.org/0953-8984/16/49/002)

INSTITUTE OF PHYSICS PUBLISHING JOURNAL OF PHYSICS: CONDENSED MATTER

J. Phys.: Condens. Matter **16** (2004) 8823–8834 PII: S0953-8984(04)87243-6

A structural study of ceramics in the $(BiMnO_3)_x$–$(PbTiO_3)_{1-x}$ solid solution series

David I Woodward and Ian M Reaney

Department of Engineering Materials, University of Sheffield, Mappin Street, Sheffield S1 3JD, UK

E-mail: d.woodward@sheffield.ac.uk

Received 4 October 2004, in final form 28 October 2004
Published 26 November 2004
Online at stacks.iop.org/JPhysCM/16/8823
doi:10.1088/0953-8984/16/49/002

Abstract

Ceramics in the $(BiMnO_3)_x$–$(PbTiO_3)_{1-x}$ series were fabricated with compositions in the range $0 < x \leqslant 0.7$. A macroscopically pseudocubic structure was observed for compositions $x > 0.4$ while at $x < 0.4$ the structure is tetragonal. The presence of a pseudocubic structure is attributed to frustration between different preferred environments of cations, leading to an absence of long-range ordered polar ionic displacements. Microstructures similar to those of relaxors were observed at $x = 0.4$ and evidence of incommensurate ordering of antiparallel cation displacements was found at compositions $x \geqslant 0.6$. Permittivity measurements for $x = 0.3$ and 0.4 revealed diffuse frequency-dependent maxima between 100 and 300 °C. In addition, compositions with $x \leqslant 0.3$ exhibited a sharp peak at higher temperature. The broad peaks are considered to arise from different time constants attributed to the grain interiors and boundaries for $x = 0.3$ and 0.4 whereas the sharp peak is interpreted as the Curie temperature of a tetragonal to cubic phase transition.

1. Introduction

The phase diagram of the $(BiFeO_3)_x$–$(PbTiO_3)_{1-x}$ solid solution contains a morphotropic phase boundary (MPB) between tetragonal and rhombohedral structures at $x \approx 0.7$ [1]. Around this composition, the tetragonal structure exhibits a large spontaneous strain reaching a maximum at the MPB, with a c/a ratio of 1.16 recently measured at $x = 0.7$ [2]. Attempts to exploit the high Curie temperature, T_C, of ∼632 °C [3] and the potentially large polarization afforded by such a large c/a ratio have been hampered by high conductivity [4] leading to difficulties with poling ceramics. The mechanism leading to the appearance of such a large c/a ratio is unknown and the question remains as to whether distortions of similar magnitude exist in other $BiMeO_3$–$PbTiO_3$ solid solutions (where Me is a trivalent cation). Recent works [5, 6]

have illustrated that $BiScO_3$–$PbTiO_3$ and $BiMg_{1/2}Ti_{1/2}O_3$–$PbTiO_3$ each have an MPB similar to that in $PbZrO_3$–$PbTiO_3$ in which the value of c/a in the tetragonal phase field decreases as the MPB is approached: an opposite trend to that in $BiFeO_3$–$PbTiO_3$. No prior investigations of ceramics in the $BiMnO_3$–$PbTiO_3$ series have been reported, although several studies have been performed on $BiMnO_3$. A recent neutron diffraction study [7] refined the structure of $BiMnO_3$ as monoclinic, with space group $C2$, resulting from the Glazer tilt system [8] $a^-b^-b^-$. Dielectric hysteresis loops were recently published, indicating the presence of ferroelectricity and x-ray diffraction (XRD) revealed a phase transition at ∼180 °C, considered to be the Curie temperature [9]. Like the Fe^{3+} ion, Mn^{3+} has a magnetic moment, but in addition, Mn^{3+} exhibits a known Jahn–Teller effect when in octahedral coordination, leading to elongation of the two axial Mn–O bonds [10]. This paper aims to test the hypothesis that coupling of the Jahn–Teller effect to a tetragonal ferroelectric distortion could enhance the spontaneous strain in the tetragonal structure close to the MPB in the $BiMnO_3$–$PbTiO_3$ solid solution.

2. Experimental details

Ceramic samples were fabricated in the $(BiMnO_3)_x$–$(PbTiO_3)_{1-x}$ series by the conventional mixed oxide route. Bi_2O_3 (99.9%, Acros Organics, Geel, Belgium), Mn_2O_3 (99.8%, Malinckrodt Baker Inc., Phillipsburg, New Jersey, USA), PbO (99.9%, Acros Organics, Geel, Belgium) and TiO_2 (99.9%, Sigma-Aldrich, Dorset, UK) were weighed out in stoichiometric amounts in batches of ∼100 g to an accuracy of 0.01 g and attrition milled for 1 h using 2 mm diameter Y_2O_3-stabilized ZrO_2 milling media in distilled water. The media were removed and the remaining slurry was dried at 80 °C for two days. The powder was collected and ground with a pestle and mortar to pass through a 355 μm mesh sieve. Powders with compositions $x < 0.7$ were reacted in air in a lidded Al_2O_3 crucible for 2 h at 850 °C with the exception of $PbTiO_3$ ($x = 0$) which was reacted at 800 °C. For powders of composition $x \geqslant 0.7$, significant sintering of the oxides took place at 850 °C rendering them hard and particularly difficult to mill. A reaction temperature of 700 °C was used for these compositions which led to a powder that was multiphase but soft enough for milling. The reacted powders were attrition milled, dried and sieved as above. Approximately 1 g of each of these powders was uniaxially pressed into pellets of 10 mm diameter with a load of ∼100 MPa and then sintered for 2 h in air on a CaO-stabilized ZrO_2 tile covered with Pt foil, beneath an upturned crucible and next to a small pile of powder with the same composition as the pellets. Sintering temperatures of between 975 and 1075 °C were used. Weight loss on sintering was found to be between 1.3% and 0.5% but no attempt was made to compensate for this loss as the evaporating species was not known. At $x > 0.6$, severe deformation of the pellets took place during sintering at 1000 °C, due to the proximity of the melting temperature. As a result, no pellets of composition $x > 0.7$ could be made with perovskite as the majority phase due to the low sintering temperatures imposed. Due to fracturing of the pellets during sintering, $PbTiO_3$ ($x = 0$) was used only as a powder.

Pellets were thermally etched for 30 min at temperatures between 900 and 1000 °C. Scanning electron microscopy (SEM) was performed on etched and unetched pellets with a JEOL JSM 6400 operating at 10 kV. Link ISIS energy dispersive spectroscopy (EDS) was incorporated into the microscope and was used with an accelerating voltage of 20 kV and a spot size of 1 nm. XRD was carried out between 10° and 70° 2θ on crushed pellets with Cu Kα radiation from a Philips PW 1373 diffractometer. Samples for transmission electron microscopy (TEM) were prepared by grinding pellets to a thickness of ∼30 μm, fixing the thinned samples to a copper ring and milling to perforation at an incidence angle of 12° with a Gatan duo ion mill (600 model) at an accelerating voltage of 6 kV and a combined gun current

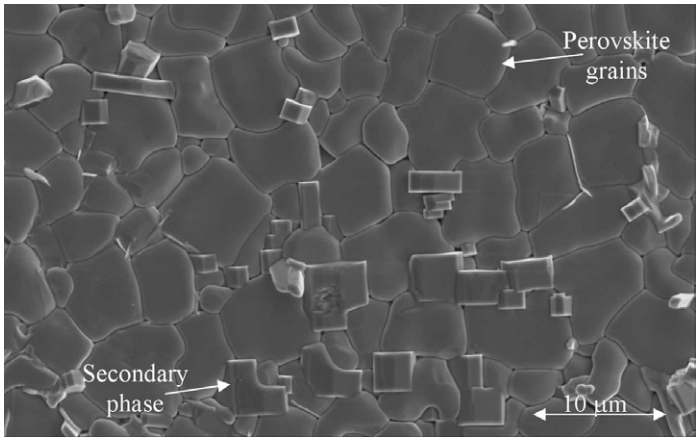

Figure 1. The thermally etched surface of an $x = 0.6$ pellet. Secondary phases, formed during the etching process, appear as rectangular particles.

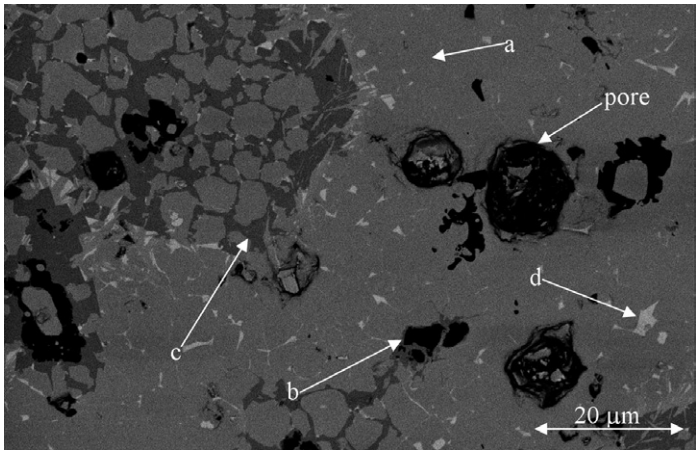

Figure 2. A backscattered scanning electron image of an $x = 0.7$ pellet. Areas of different composition are labelled (a–d) and correspond to EDS spectra (a–d) in figure 3.

of 0.6 mA. An FEI Tecnai 20 operating at 200 kV was used to analyse these samples. Gold electrodes were applied to pellets as a paste and fired at 850 °C. Pellets were placed in a tube furnace and heated to 600 °C at a rate of 1 K min^{-1} while permittivity measurements were performed using an HP 4284A Precision LCR meter.

3. Results and discussion

3.1. SEM

Figure 1 shows a thermally etched $x = 0.6$ pellet illustrating the density, grain size and shape typical of pellets in this series. Perovskite grains are between 1 and 10 μm in width and have no preferred growth direction. The observed porosity is low, consistent with the sintered density >95% of the theoretical density (8.22 g cm^{-3}). All pellets contained secondary phases although their presence was only detected by means of XRD in pellets of composition $x \geqslant 0.7$. Figure 2 shows the presence and distribution of three secondary phases in an $x = 0.7$ pellet. EDS spectra indicated that these additional phases are forms of manganese and bismuth oxide and an oxide apparently rich in both Mn and Bi (figure 3). Areas of Mn and Bi oxides have been observed in pellets of all compositions within this series although in much smaller proportions than those shown in figure 2.

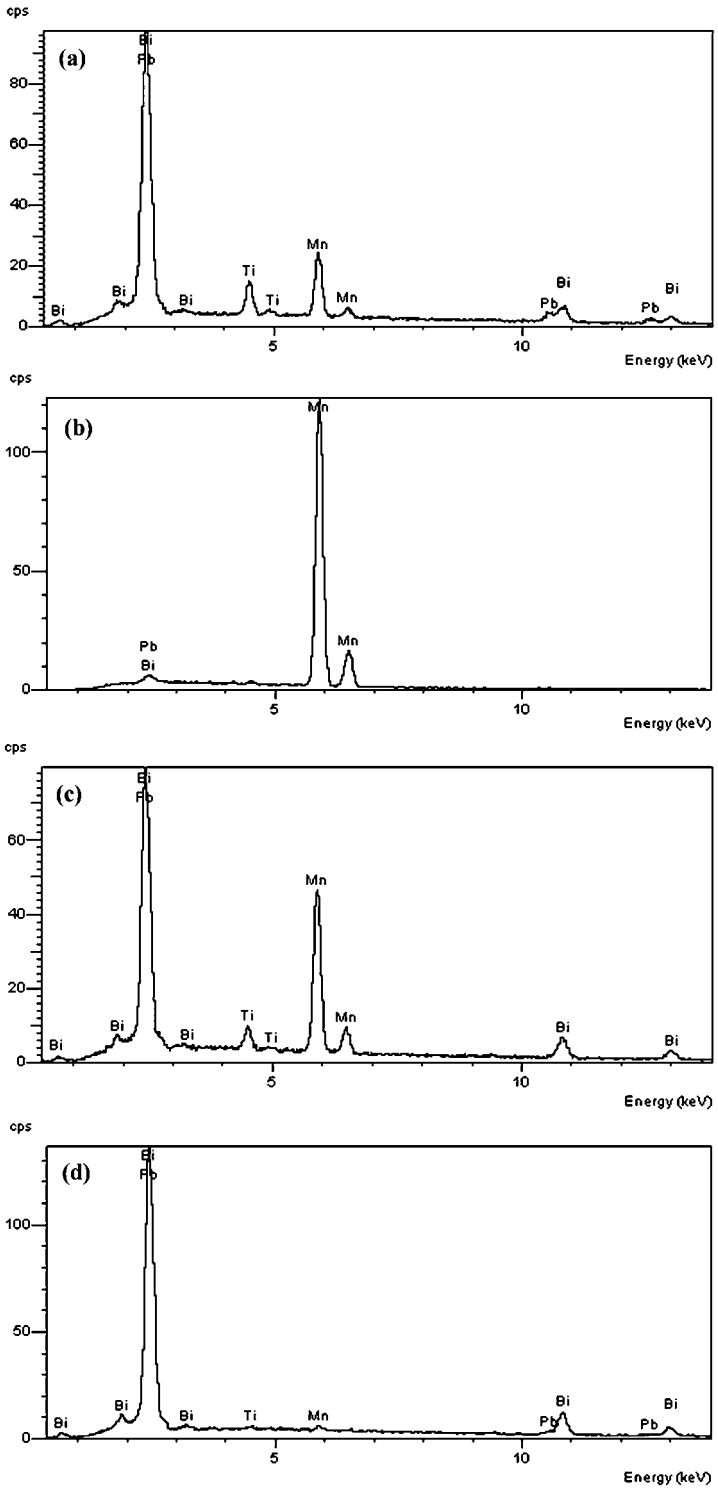

Figure 3. EDS spectra from (a) perovskite and ((b)–(d)) secondary phases present in an $x = 0.7$ pellet and indicated in figure 2.

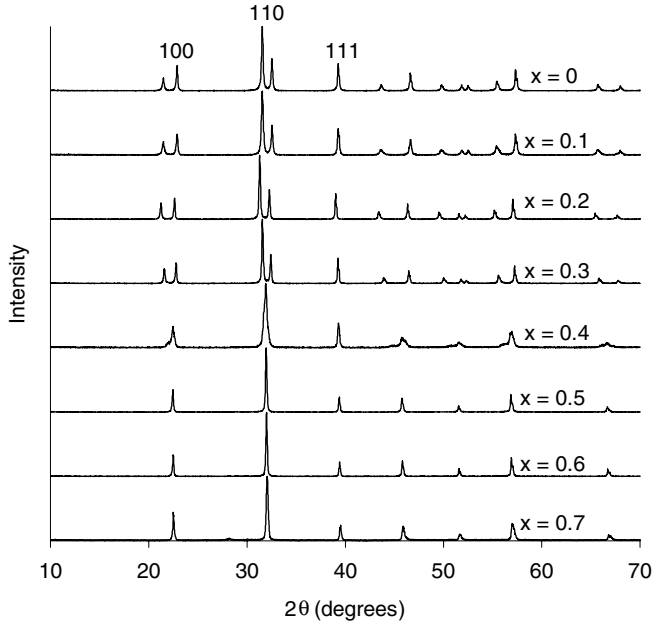

Figure 4. XRD traces obtained from crushed pellets of selected compositions in the $(BiMnO_3)_x$–$(PbTiO_3)_{1-x}$ series.

3.2. XRD

XRD traces from crushed pellets in the $(BiMnO_3)_x$–$(PbTiO_3)_{1-x}$ series are shown in figure 4. Samples with $x < 0.7$ exhibited only perovskite peaks. Traces obtained from $x = 0.7$ pellets contain reflections corresponding to secondary phases but these were too weak in intensity to unambiguously identify the phases present. Splitting of pseudocubic {100} and {110} perovskite peaks, consistent with tetragonal symmetry, was observed for $x < 0.4$. No splitting of any peaks was observed for powders of composition $x > 0.4$, indicating a cubic or pseudocubic structure. At $x = 0.4$, some asymmetry of {100} and {110} peaks was taken to be an indication of slight tetragonal distortion. Based on these observations, a phase boundary may be inferred, between tetragonal and pseudocubic phases, for $0.4 < x < 0.5$. Lattice parameters were fitted to the XRD traces and their dependence on composition is shown in figure 5. The enhanced spontaneous strain, expected as a result of Jahn–Teller and ferroelectric distortion coupling, does not appear and it is concluded that these distortions do not couple, but frustrate, leading to minimal overall distortion and a structure that is pseudocubic.

3.3. TEM

Figure 5 shows domain structures obtained from thinned samples with compositions $x = 0.3$, 0.4 and 0.5. The image obtained at $x = 0.3$ (figure 6(a)) contains lamellar domains that are consistent with twinning arising from the tetragonal distortion apparent in the XRD trace in figure 2. Samples with composition $x = 0.5$ (figure 6(c)) showed no lamellar domain structure, consistent with a pseudocubic structure. Samples with composition $x = 0.4$ (figure 6(b)) exhibited a mottled contrast and regions of fine-scale striations. Similar structural features have been observed in La-doped lead zirconate titanate (PLZT) ceramics in a narrow compositional region separating a tetragonal ferroelectric phase from a paraelectric phase [11]. It was found that as the La concentration decreased from ∼15 mol%, the generally featureless grains of the cubic phase were replaced with a fine-scale (∼5 nm) mottled contrast, associated with a relaxor

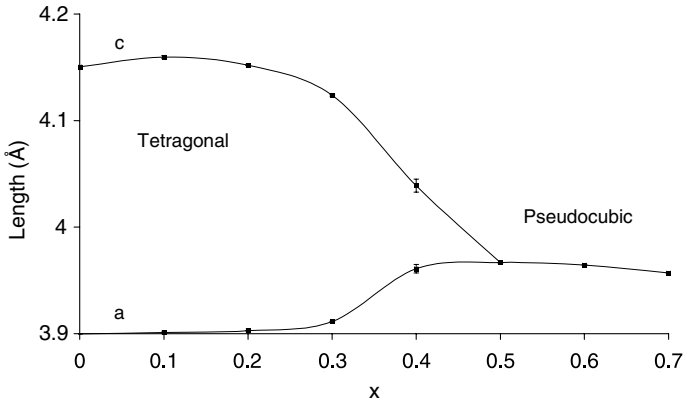

Figure 5. The composition dependence of the lattice parameters fitted to XRD traces in figure 4.

phase. As the ferroelectric phase was approached, the mottling gave way to striations with a similarly fine scale of ∼20 nm, and finally to long-range ordered macrodomains typical of a tetragonally distorted structure. Here, it is proposed that the mottled contrast seen in figure 6(b) indicates the existence of a short-range ordered polar phase similar to a relaxor between the pseudocubic ($x = 0.5$) and tetragonal ($x = 0.3$) phases. The presence of striations within the same sample suggests that, due to the heterogeneity present in the pellets, some areas have a local composition approaching that of the tetragonal phase. Taking into account the absence of lamellar domains in the microstructure, as observed by TEM, it is concluded that the structure at this composition is primarily not tetragonal as implied by the XRD, but pseudocubic. The slight splitting and asymmetry of the peaks observed in the XRD spectrum (figure 3) may be due to diffraction from areas with the striated microstructure.

Zone axis diffraction patterns (ZADPs) were obtained from principal zone axes at all compositions and at $x < 0.6$ exhibited reflections entirely consistent with a simple cubic perovskite lattice (figures 7(a) and (d)). However, for $x = 0.6$ and 0.7 samples, incommensurate superstructure reflections were found in $\langle 100 \rangle_p$ and $\langle 111 \rangle_p$ but not $\langle 110 \rangle_p$ ZADPs (where the subscript 'p' indicates reference to the pseudocubic cell) (figures 7(b), (c), (e) and (f)). These reflections were found at $y\{ooe\}_p$ positions (where 'o' and 'e' refer to odd and even miller indices, respectively and y is a fraction in the range $\frac{1}{4} < y < \frac{1}{3}$). At $x = 0.6$, these reflections are diffuse and streaked, suggesting significant variation in long-range order, but at $x = 0.7$ the reflections are discrete. The fact that y is not an integer fraction means that the superstructure responsible is incommensurate in nature and cannot be the result of a commensurate octahedral tilting phase transition. Also unlikely is the positional ordering of cations or oxygen vacancies since, by definition, the corresponding reflections must lie on commensurate lattice points. Similar incommensurate reflections have been observed in ordered complex perovskites such as $PbCo_{1/2}W_{1/2}O_3$ (PCW) and $PbSc_{1/2}Ta_{1/2}O_3$ (PST) [12] and in systems such as La-doped $PbZr_{0.9}Ti_{0.1}O_3$ (PLZT) [13] at compositions close to an antiferroelectric/ferroelectric (AFE/FE) phase boundary. These reflections are associated with incommensurate antiparallel cation displacements [14] and in PLZT, PCW and PST result in the appearance of satellite reflections that lie along the $\langle 110 \rangle_p$ directions that are often streaked. These reflections are found to be present in the $\langle 111 \rangle_p$ and $\langle 001 \rangle_p$ but not $\langle 110 \rangle_p$ zone axes, since the related AFE commensurate phases (e.g. $PbZrO_3$ in the case of PLZT) have structures in which $\frac{1}{4}\{hk0\}_p$ superlattice reflections are allowed but only where $h \neq k$. Since only $\frac{1}{4}\{hk0\}_p$ where $h = k$ reflections are allowed in $\langle 110 \rangle_p$ zone axes by the Weiss zone law, the incommensurate reflections are not observed. Comparison of

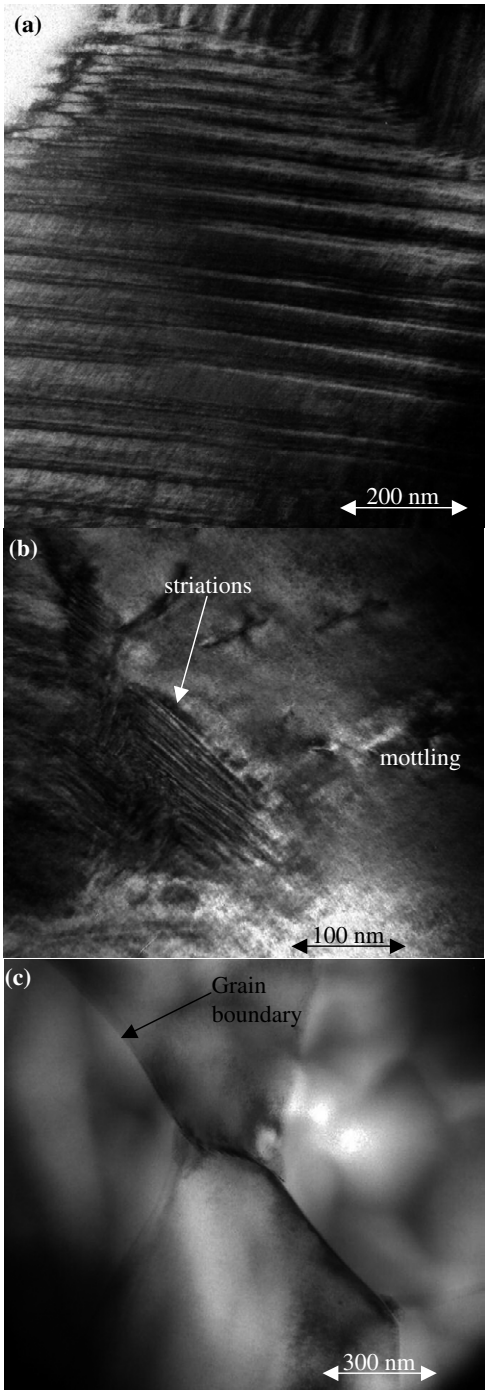

Figure 6. Bright field TEM micrographs showing typical features of samples with compositions (a) $x = 0.3$, (b) $x = 0.4$ and (c) $x = 0.5$. Key features are indicated.

the incommensurate reflections in this sample with those in PLZT, PST and PCW reveals that these intensities are more diffuse, indicating that the mechanism responsible does not have long-range coherence. Moreover, it is postulated that the presence of the superstructure may

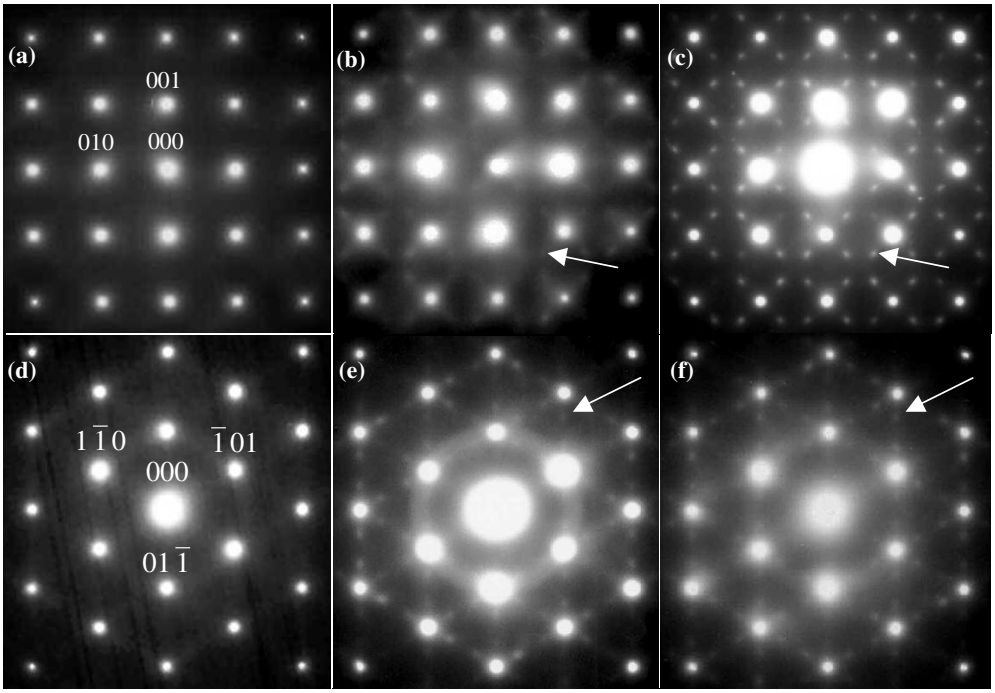

Figure 7. ((a)–(c)) $\langle 100 \rangle_p$ ZADPs from samples of the $(BiMnO_3)_x$–$(PbTiO_3)_{1-x}$ series; (a) $x = 0.5$, (b) $x = 0.6$ and (c) $x = 0.7$. ((d)–(f)) $\langle 111 \rangle_p$ ZADPs from the same. Superstructure reflections are arrowed.

indicate that $x = 0.7$ lies close to an AFE/FE phase boundary. This composition represents the solubility limit of $BiMnO_3$ in $PbTiO_3$ at ambient pressure, before samples become excessively multiphase. Therefore, the $BiMnO_3$ concentration cannot be further increased to study the evolution of the superstructure reflections as a function of composition. However, $BiMnO_3$ is not known to be antiferroelectric [9] and simulations of diffraction patterns using the structure refined by Atou *et al* [7] do not indicate the presence of any superstructure reflections in either $\langle 100 \rangle_p$ or $\langle 111 \rangle_p$ zone axis diffraction patterns.

EDS and electron diffraction were used to identify secondary phases in some of the compositions. The presence of hausmannite, Mn_3O_4, was confirmed in $x = 0.4$ and 0.6 samples (figure 8), while braunite, $Mn_7O_8{\cdot}SiO_4$, was found in the $x = 0.5$ sample (figure 9). Both identified structures contain Mn^{3+} and Mn^{2+} ions and it is inferred that both valence states are thermodynamically able to exist in the perovskite lattice under the sintering conditions.

3.4. Dielectric properties

Figure 10 shows the temperature dependences of the relative permittivity for $x = 0.4$ and 0.3 pellets across a range of frequencies. In the plot for $x = 0.4$ (figure 10(a)), the strong frequency dependence of T_m is similar to that of a relaxor ferroelectric. However, the curves differ so markedly across the entire temperature range that conventional relaxor behaviour is probably not responsible for the frequency dependence observed. A feature common to ceramics is the difference in frequency response between the grain interiors (or bulk) and boundaries. The bulk exhibits a maximum response at higher frequencies than the grain boundaries, due to the inherent capacitance determined by their respective geometries [17]. Thus, the temperature-

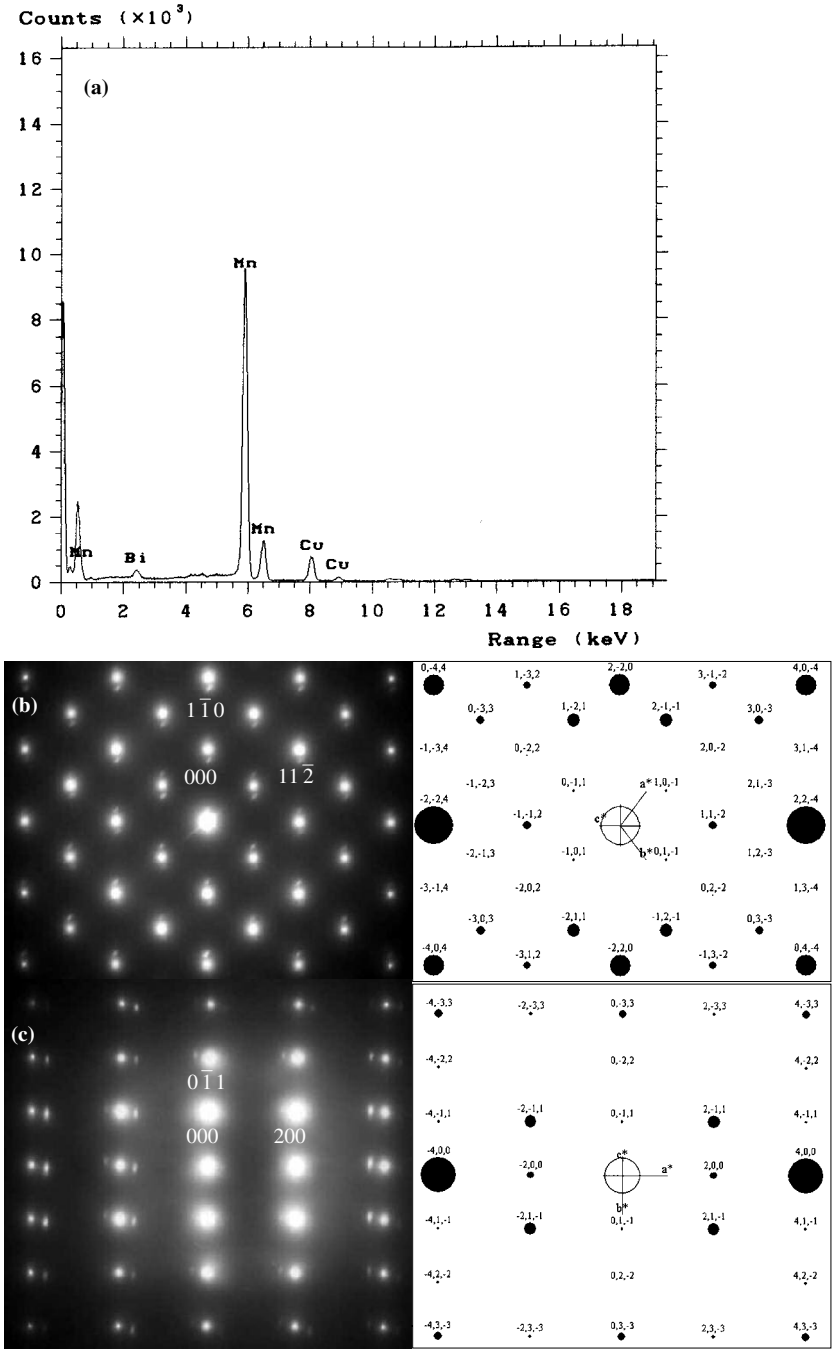

Figure 8. (a) An EDS spectrum from the secondary phase in an $x = 0.4$ sample with electron diffraction patterns matched to (b) [111] and (c) [011] ZADPs from hausmannite, Mn_3O_4 (PDF 24-734). Lattice parameters and atomic positions published by Jarosh [15] were used to create the simulations. Cu peaks in the EDS spectrum originate from the supporting copper ring and Bi peaks originate from the adjacent perovskite phase.

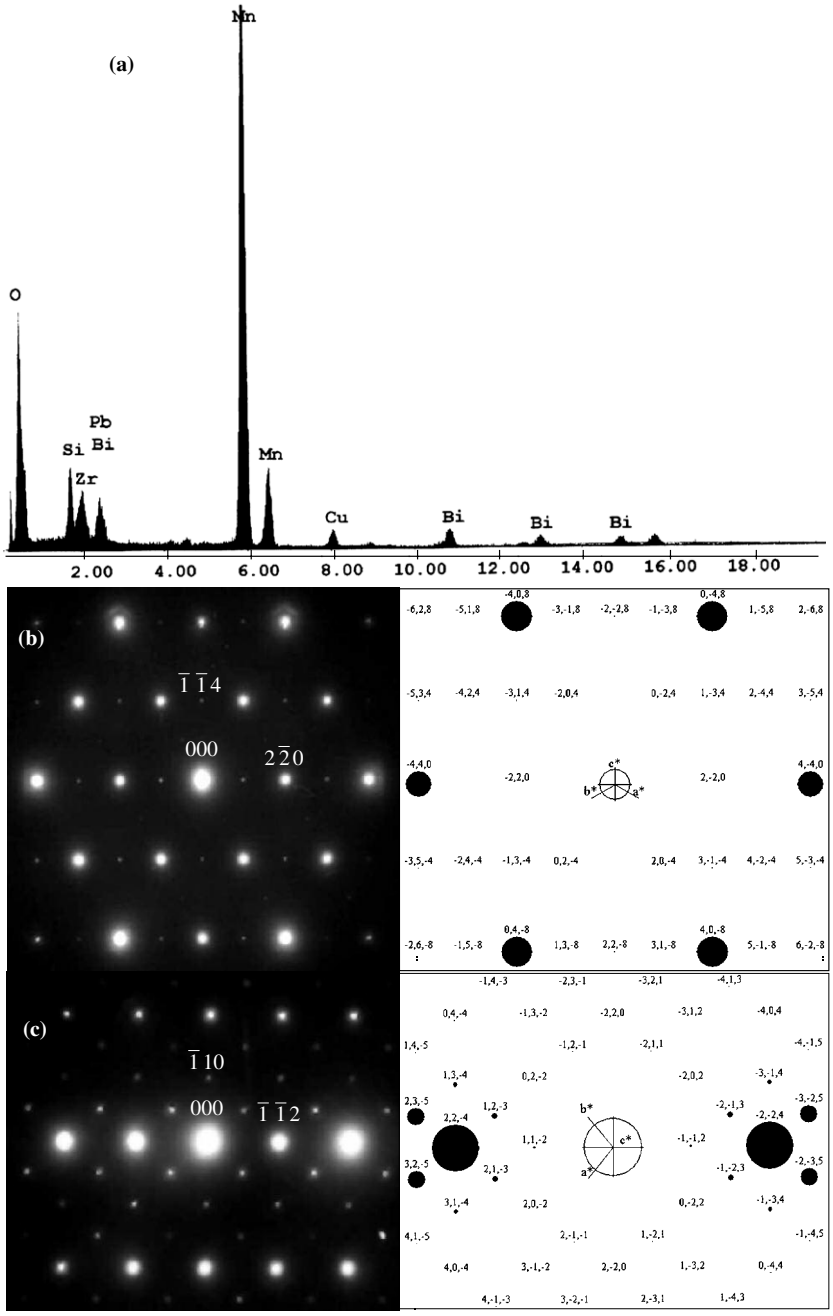

Figure 9. (a) An EDS spectrum from the secondary phase in an $x = 0.5$ sample with electron diffraction patterns matched to (b) [221] and (c) [111] ZADPs from braunite, $Mn_7O_8{\cdot}SiO_4$. Lattice parameters and atomic positions published by Moore and Araki [16] were used to create the simulations. Cu peaks in the EDS spectrum originate from the supporting copper ring and Bi peaks originate from the adjacent perovskite phase.

dependent plots of permittivity in figure 10(a) may show only a combination of reduced grain boundary and bulk ceramic response. Figure 10(b) shows the permittivity data encountered

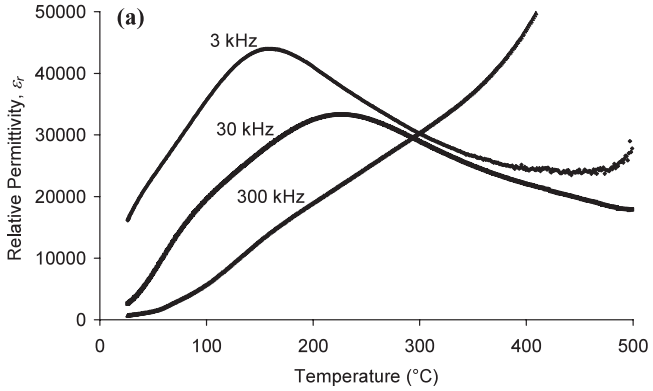

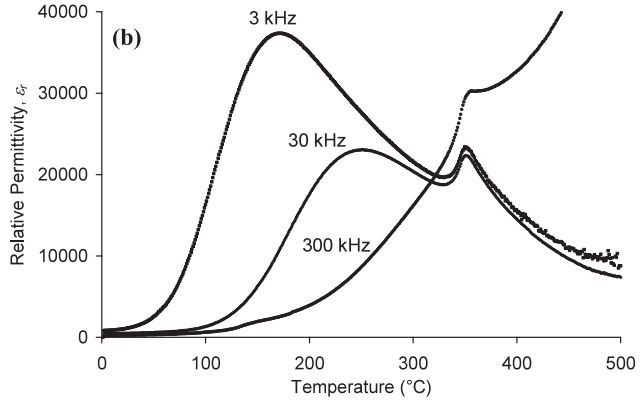

Figure 10. The frequency dependence of permittivity versus temperature plots for pellets of composition (a) $x = 0.4$ and (b) $x = 0.3$.

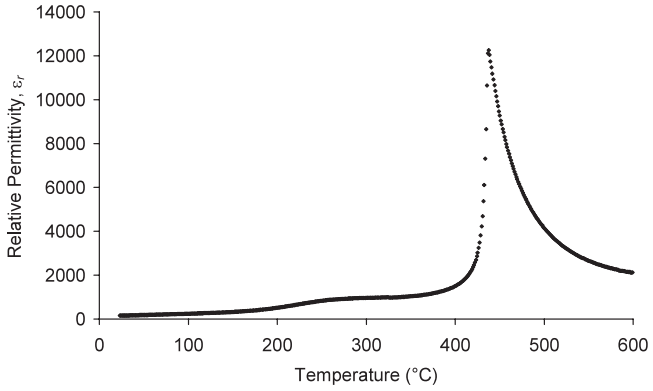

Figure 11. Permittivity versus temperature for a pellet of composition $x = 0.2$ at 30 kHz.

at $x = 0.3$. The strongly frequency-dependent behaviour of the permittivity at temperatures $<400\,^{\circ}C$ is similar to that recorded for the pellet with composition $x = 0.4$ and may also arise from the progression from a grain boundary dominated response at lower frequencies to a bulk response at higher frequencies. A frequency-independent, local maximum in permittivity is observed at $T_m \approx 355\,^{\circ}C$, indicative of a phase transition. This is consistent with the expected T_C for this composition, given that the T_Cs of the two end-members are $\sim$180 and 490 °C for $BiMnO_3$ and $PbTiO_3$, respectively, and assuming a roughly linear change in T_C with x. This peak is likely to arise from the observed tetragonal regions illustrated in figure 6(a).

Fixed-frequency measurements indicate that T_C increases as x decreases for samples where $x \leqslant 0.3$ (figure 11), as expected. The absence of a similar peak from the permittivity data obtained at $x = 0.4$ is further evidence of the presence of a pseudocubic structure for this composition. Although further studies of the dielectric response over a broad frequency and temperature range could unambiguously determine the nature of the broad maxima for $x = 0.3$ and 0.4, the evidently high conductivity and apparent absence of a rhombohedral–tetragonal phase boundary preclude any practical applications for these ceramics.

4. Conclusions

The limit of solid solution for the $(BiMnO_3)_x$–$(PbTiO_3)_{1-x}$ system under the processing conditions employed was $x = 0.7$. Pellets with compositions $x \geqslant 0.4$ were found, against expectations, to have a macroscopically pseudocubic structure, despite the Jahn–Teller distortion associated with Mn^{3+} ions in octahedral coordination. A frustration effect arising from the different preferred environments of the cations, resulting in the absence of long-range coupling of ionic displacements, is proposed to account for the pseudocubic structure. At $x < 0.4$, samples have a tetragonal structure.

For $(BiMnO_3)_x$–$(PbTiO_3)_{1-x}$ samples at $x = 0.4$, the microstructure exhibited similarities to relaxor phases, consistent with the absence of long-range ordered ionic displacements. In samples with compositions $x = 0.6$ and 0.7, close to the limit of solubility, a superstructure associated with incommensurate ordering of antiparallel cation displacements is thought to be present.

Acknowledgment

The authors would like to thank the EPSRC for funding (Grant No GR/S60037/01).

References

[1] Venevtsev Y N, Zhdanov G S, Solov'ev S N, Bezus E V, Ivanova V V, Fedulov S A and Kapyshev A G 1960 *Sov. Phys.—Crystallogr.* **5** 594
[2] Woodward D I, Reaney I M, Eitel R E and Randall C A 2003 *J. Appl. Phys.* **94** 3313
[3] Sai Sunder V V S S, Halliyal A and Umarji A M 1995 *J. Mater. Res.* **10** 1301
[4] Fedulov S A, Venevtsev Y N, Zhdanov G S, Smazhevskaya E G and Rez I S 1962 *Sov. Phys.—Crystallogr.* **7** 62
[5] Eitel R E, Randall C A, Shrout T R, Rehrig P W, Hackenberger W and Park S-E 2001 *Japan. J. Appl. Phys.* **40** 5999
[6] Randall C A, Eitel R, Jones B, Shrout T R, Woodward D I and Reaney I M 2004 *J. Appl. Phys.* **95** 3633
[7] Atou T, Chiba H, Ohoyama K, Yamaguchi Y and Syono Y 1999 *J. Solid State Chem.* **145** 639
[8] Glazer A M 1972 *Acta Crystallogr.* B **28** 3384
[9] Moreira dos Santos A, Parashar S, Raju A R, Zhao Y S, Cheetham A K and Rao C N R 2002 *Solid State Commun.* **122** 49
[10] Proffen T, DiFrancesco R G, Billinge S J L, Brosha E L and Kwei G H 1999 *Phys. Rev.* B **60** 9973
[11] Akbas M A, Reaney I M and Lee W E 1996 *J. Mater. Res.* **11** 2293
[12] Randall C A, Markgraf S A, Bhalla A S and Baba-Kishi K 1989 *Phys. Rev.* B **20** 413
[13] Knudsen J, Woodward D I and Reaney I M 2003 *J. Mater. Res.* **18** 262
[14] Baba-Kishi K Z and Barber D J 1990 *J. Appl. Crystallogr.* **23** 43
[15] Jarosh D 1987 *Miner. Petrol.* **37** 15
[16] Moore P B and Araki T 1976 *Am. Mineral.* **61** 1226
[17] Irvine J T S, Sinclair D C and West A R 1990 *Adv. Mater.* **2** 132